Title: 2-Methyl-β-cyclodextrin grafted ammonium chitosan: synergistic effects of cyclodextrin host and polymer backbone in the interaction with amphiphilic prednisolone phosphate salt as revealed by NMR spectroscopy
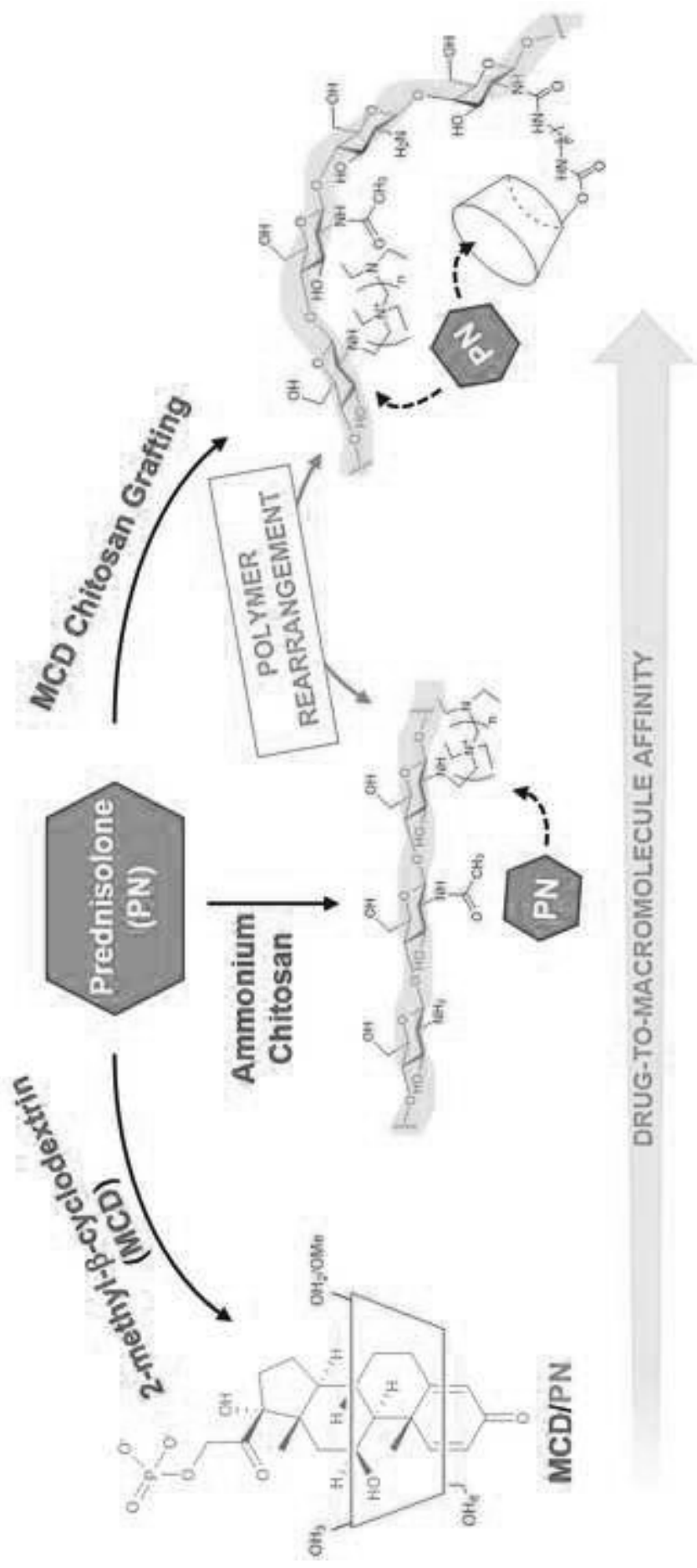
Corresponding Author: Dr. Federica Balzano, Ph.D.

Corresponding Author's Institution: University of Pisa

First Author: Andrea Cesari

Order of Authors: Andrea Cesari; Anna Maria Piras; Ylenia Zambito; Gloria Uccello Barretta; Federica Balzano

Abstract: Reduced molecular weight chitosan was quaternized with 2-chloro-N,N-diethylethylamine to obtain a water soluble derivative (N+-rCh). Methylated-β-cyclodextrin (MCD), with 0.5 molar substitution, was covalently linked to N+-rCh through 1,6-hexamethylene diisocyanate spacer to give the derivatized ammonium chitosan N+-rCh-MCD. To shed light on the role of the cyclodextrin pendant in guiding binding interactions with amphiphilic active ingredients, corticosteroid prednisolone phosphate salt (PN) was considered. The deep inclusion of PN into cyclodextrin in PN/MCD model system was pointed out by analysis of 1H NMR complexation shifts, 1D ROESY spectra, and diffusion measurements (DOSY). By using proton selective relaxation rates measurements as investigation tool, the superior affinity of N+-rCh-MCD towards PN was demonstrated in comparison with parent ammonium chitosan N+-rCh.

Prednisolone (PN)

2-methyl-β-cyclodextrin (MCD)

MCD Chitosan Grafting

Ammonium Chitosan

POLYMER REARRANGEMENT

PN

PN

MCD/PN

DRUG-TO-MACROMOLECULE AFFINITY

1    **2-Methyl-β-cyclodextrin grafted ammonium chitosan: synergistic effects of cyclodextrin**

2    **host and polymer backbone in the interaction with amphiphilic prednisolone phosphate**

3    **salt as revealed by NMR spectroscopy**

4

5    Andrea Cesari[a], Anna Maria Piras[b], Ylenia Zambito[b], Gloria Uccello Barretta[a], and Federica

6    Balzano[a],*

7

8    [a]Department of Chemistry and Industrial Chemistry, University of Pisa, via Moruzzi 13, 56124 Pisa, Italy.

9    [b]Department of Pharmacy, University of Pisa, via Bonanno 33, 56126 Pisa, Italy.

10    *Corresponding author *E-mail addresses: [federica.balzano@unipi.it](federica.balzano@unipi.it)*.

11

12    **Abstract**

13    Reduced molecular weight chitosan was quaternized with 2-chloro-*N,N*-diethylethylamine to obtain a

14    water soluble derivative ($N^+$-rCh). Methylated-β-cyclodextrin (MCD), with 0.5 molar substitution,

15    was covalently linked to $N^+$-rCh through 1,6-hexamethylene diisocyanate spacer to give the

16    derivatized ammonium chitosan $N^+$-rCh-MCD. To shed light on the role of the cyclodextrin pendant

17    in guiding binding interactions with amphiphilic active ingredients, corticosteroid prednisolone

18    phosphate salt (PN) was considered. The deep inclusion of PN into cyclodextrin in PN/MCD model

19    system was pointed out by analysis of $^1H$ NMR complexation shifts, 1D ROESY spectra, and

20    diffusion measurements (DOSY). By using proton selective relaxation rates measurements as

21    investigation tool, the superior affinity of $N^+$-rCh-MCD towards PN was demonstrated in comparison

22    with parent ammonium chitosan $N^+$-rCh.

23

24    **Keywords**

## 1.  Introduction

Polysaccharides play a leading role in the design of suitable platforms for the targeted and controlled release of active ingredients. As a matter of fact, polysaccharides have low production costs, negligible toxicity and desirable pharmaceutical properties, such as high biocompatibility, antimicrobial activity, and bioadhesive properties (Miao et al., 2018). Chitin is the second most abundant polysaccharide found in nature, and its partially deacetylated form, namely chitosan (Ch, Figure 1), has been one of the main focus in biomedical applications (Dash et al., 2011). Ch, differently from its parent compound, is soluble in acidic aqueous medium (pH<6) due to protonation of the deacetylated amino groups (Sogias et al., 2010). However, very high-molecular weight chitosan may lead to highly viscous solutions, which can be detrimental for some pharmaceutical applications. For this reason, degradation of chitosan to a reduced molecular weight (rCh) may be a first beneficial modification. In order to improve Ch solubility at physiological pH, several chemical modifications have been proposed (Zhang et al., 2010). Nucleophilic reactivity of -NH$_2$ and -OH groups in Ch constituting units (Figure 1) can be exploited for covalent bonds formation, as in the case of the introduction of amino-alkylated chains into rCh backbone by using 2-chloro-*N,N*-diethylethylamine to produce an ammonium alkylated chitosan (N$^+$-rCh, Figure 1) with improved aqueous solubility in a wide range of pH. The product shows enhanced antibacterial and mucosal permeation promoting properties (Zambito et al., 2008).

In the area of controlled drug release, aggregation of Ch or its derivatives into nanoparticulated forms leads to relevant advantages in terms of drug bioavailability and affinity (Cesari et al., 2020a; Fabiano et al., 2018). However, the production of nanoparticles requires standardization of experimental procedures for the accurate control of sizes, polydispersity and stability of the final particles (Sreekumar et al., 2018).

51    An alternative attractive method to enhance drug-to-polymer affinity is represented by the use of

52    cyclodextrin-grafted chitosans. Cyclodextrins are cyclic oligosaccharides disposed in a toroidal

53    geometry, with a central hydrophobic cavity able to include apolar guest molecules, but

54    simultaneously promoting hydrophilic interactions at their external polar surface. Besides native

55    cyclodextrins (α-CD, β-CD, and γ-CD, constituted by 6, 7, or 8 glucose units, respectively), different

56    CD derivatives have made their entry into the pharmaceutical market due to their enhanced water

57    solubility, as in the case of randomly methylated β-CD (>500 mg/mL, 25 °C) (Saokham et al., 2018).

58    In fact, the methylation of hydroxylic groups of CD breaks the network of intra-molecular hydrogen

59    bonds between -OH groups and prevents crystallization by producing a statistically substituted and

60    amorphous product (Davis and Brewster, 2004). Moreover, aliphatic groups make the internal surface

61    of CD cavity more hydrophobic, favouring the inclusion of lipophilic molecules. The covalent

62    conjugation of cyclodextrins to the backbone of $N^+$-rCh plays a specific role, which goes beyond the

63    properties of the simple physical mixture CD/$N^+$-rCh. Recently, we have investigated the release

64    properties of a (2-methyl-β-cyclodextrin)-grafted ammonium chitosan ($N^+$-rCh-MCD, Figure 1) as a

65    polymeric scaffold for hydrophilic active ingredient: accurate NMR investigations highlighted

66    synergistic effects between the covalently linked macrocyclic oligosaccharide and the polymeric

67    chains (Cesari et al., 2020b).

68
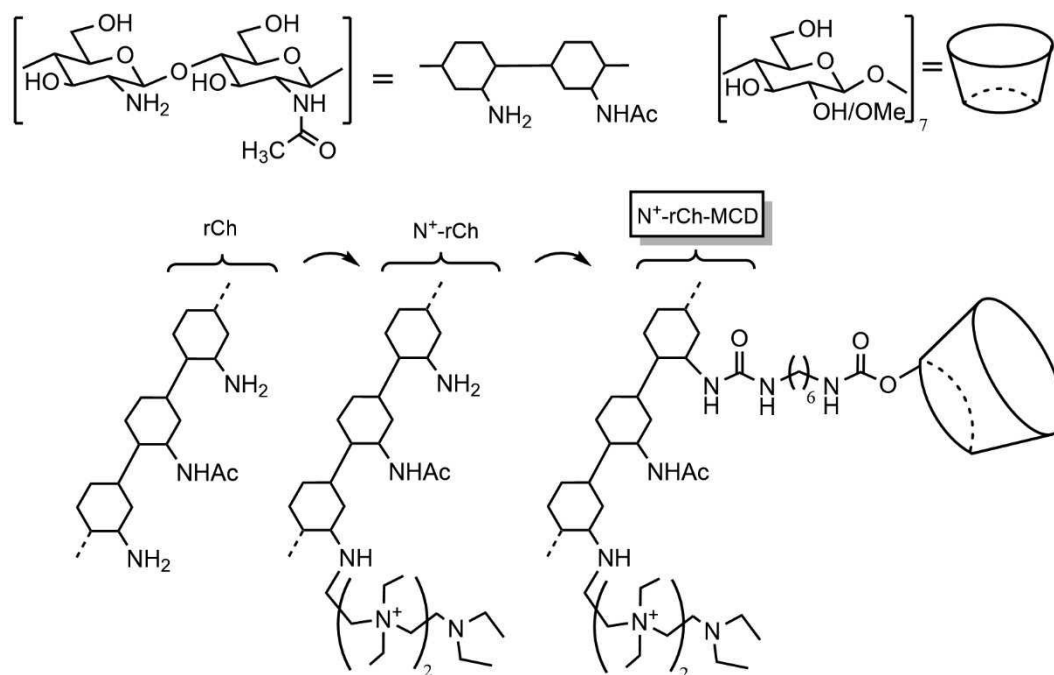
69 Figure 1. Chemical structure of reduced molecular weight chitosan (rCh), ammonium alkylated

70 chitosan (N⁺-rCh) and (2-methyl-β-cyclodextrin)-grafted ammonium chitosan N⁺-rCh-MCD.

71

72 N⁺-rCh-MCD also demonstrated mucoadhesive properties, simultaneously enhancing solubilization of

73 active ingredients with a high hydrophobic component (Piras et al., 2018b). Interestingly, the use of

74 nanoparticles derived from the same polymer did not seem to offer significant advantages, in terms of

75 apparent permeabilities across excised intestine (Piras et al., 2018a).

76 To evaluate the versatility of N⁺-rCh-MCD polymeric system, we focused here on prednisolone

77 phosphate salt (PN, Figure 2), i.e. an amphiphilic active ingredient simultaneously endowed with an

78 extended lipophilic skeleton and an appended polar arm. PN is a synthetic glucocorticoid with anti-

79 inflammatory and immunomodulating properties, used in a wide spectrum of medical conditions

80 (Rautio et al., 2008).

81 With this aim we carried out a detailed NMR investigation in which binding affinities of PN towards

82 N⁺-rCh-MCD, the parent polymer N⁺-rCh, and the MCD/N⁺-rCh physical mixture have been

83 compared. The stereochemical features of the model PN/MCD complex have been carefully

84 investigated to bring to light the role of the cyclodextrin host as the key component able to exert

85 possible cooperative effects with the polymeric backbone enhancing binding propensity of chitosans.

86 NMR methods of detection of through space dipole-dipole interactions, translational diffusion

87 coefficients and proton selective relaxation rates have been extensively employed to evaluate

88 stereochemical and dynamic features of supramolecular aggregates.
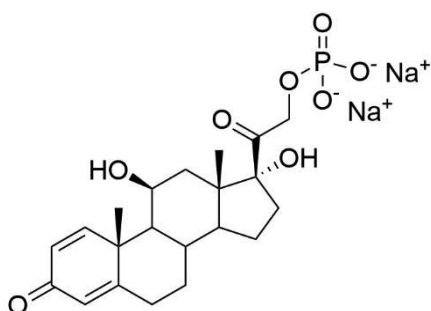


89

90 Figure 2. Prednisolone phosphate sodium salt.

91

## 2. Materials and methods

*2.1. Materials*

94 Chitosan (molecular weight = 300 kDa, food grade) was purchased from Faravelli (Milan, Italy).

95 Sodium nitrite (>97%), 2-chloro-*N*,*N*-diethylethylamine hydrochloride (DEAE-Cl·HCl, 99%),

96 dimethyl sulfoxide (DMSO), 1,6-hexamethylene diisocyanate (HMDI, ≥99.0%, freshly distilled), and

97 triethylamine (TEA, ≥ 99.5%, freshly distilled), tetramethylsilane (TMS, ≥99.5%) were purchased

98 from Sigma-Aldrich (St. Louis, MO, USA). 2-Methyl-β-cyclodextrin (MCD, MS=0.5, moisture

99 content max 5%) was purchased from Roquette (Lestrem, France). Prednisolone sodium phosphate

100 (>98%) was purchased from Tokyo Chemical Industry (Zwijndrecht, Belgium). Deuterated water

101 (D$_2$O, 99.90%) was purchased from Deutero GmbH (Kastellaun, Germany). Reduced molecular

102 weight chitosan (rCh, 134 kDa), ammonium alkylated-chitosan (N$^+$-rCh, 184 kDa) and cyclodextrin-

103      ammonium conjugated chitosan (N$^+$-rCh-MCD) were prepared according to a previously reported

104      procedure (Cesari et al., 2020b).

105      *2.2. NMR experiments*

106      NMR measurements were performed on Varian INOVA600 spectrometer (Varian Inc., Palo Alto, CA,

107      USA) operating at 600 MHz for $^1$H. The spectra are referenced through the solvent lock ($^2$H) signal

108      according to IUPAC recommended secondary referencing method. The temperature was controlled to

109      25±0.1 °C through Varian control unit. 2D NMR spectra were obtained by using standard sequences.

110      Spectral width used was the minimum required in both dimensions. 2D gCOSY (gradient COrrelated

111      SpectroscopY) spectra were recorded in the absolute mode acquiring 8 scans with a 1 s relaxation

112      delay between acquisitions and 4k data points for each of 200 FIDs. 2D TOCSY (TOtal Correlation

113      SpectroscopY) spectra were recorded acquiring 8 scans with a 1 s relaxation delay, 200 increments,

114      4k data points and a mixing time of 120 ms. 2D gHSQC (gradient Heteronuclear Single Quantum

115      Coherence) spectra were obtained with 1.2 s relaxation delay and 128 scans for each of the 128

116      increments. 1D ROESY spectra were recorded with a mixing time of 0.3 s, a delay of 1 s, and 1024

117      scans. Longitudinal selective relaxation times ($T_1^{ms}$) were measured in the initial rate approximation

118      (Freeman and Wittekoek, 1969) with standard inversion recovery pulse sequence (180°-t-90°)$_n$ using a

119      selective π-pulse calibrated at the selected frequency and a relaxation delay of 1-10 s. DOSY

120      (Diffusion Ordered SpectroscopY) experiments were carried out by using a stimulated echo sequence

121      with self-compensating gradient schemes and 64k data points. In particular, gradient strength was

122      varied in 15 steps (16 transients each), delays Δ and δ were optimized in order to obtain an

123      approximately 90% decrease in the resonance intensity at the largest gradient amplitude. The

124      baselines of all arrayed spectra were corrected prior to processing the data. After data acquisition,

125      each FID was apodized with 1.0 Hz line broadening and Fourier transformed. Gradient amplitudes in

126      DOSY experiments have been calibrated by using a standard sample of $D_2O$ 99% ($19 \times 10^{-10}$ $m^2 s^{-1}$).

127      TMS was used as viscosity reference (0.03% in $D_2O$/DMSO 95:5).

128      *2.3. Sample preparations*

129    All mixtures employed for NMR studies were prepared by mixing appropriate amounts of stock

130    solutions ($D_2O$) of each component. PN/MCD mixtures did not require specific solubilization

131    protocols. PN/N$^+$-rCh, PN/N$^+$-rCh-MCD, and PN/N$^+$-rCh/MCD mixtures were prepared as follows:

132    appropriate amounts of modified chitosan were dispersed in $D_2O$ and mixed (vortex, 600 rpm) for 2

133    hours at 40 °C. After 1 hour at room temperature, PN or PN/MCD was added to the solution and

134    stirred (600 rpm) for further 2 hours at 25 °C. Finally, samples were kept for 2 additional hours

135    without stirring and then analysed.

136

137    **3.   Results and Discussion**

138    *3.1. NMR methods*

139    Equation (1) describes the complexation equilibrium involving a low molecular weight ligand (*L*) and

140    a macromolecule (*M*).

141    $$L + M \rightleftarrows LM \qquad\qquad (1)$$
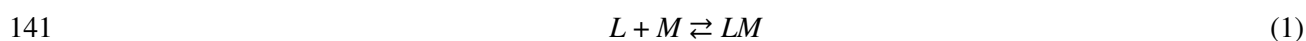
142    In fast-exchange conditions, a single set of observable NMR parameters ($P_{obs}$) is obtained and

143    represents the weighted average of the parameters in the free ($P_f$) and bound ($P_b$) states (Eq. (2)):

144    $$P_{obs} = \chi_f P_f + \chi_b P_b \qquad\qquad (2)$$

145    where $\chi_f$ and $\chi_b$ are the molar fractions of *L* in the free and bound states, respectively.

146    Since the molecular weights of ligands and macromolecules are remarkably different, very high

147    ligand-to-receptor molar ratios must be set in order to obtain observable signals for the small

148    molecule. In these experimental conditions, a significant relative weight in Eq. (2) is played by the

149    ligand in free state ($\chi_f \gg \chi_b$), and hence changes in $P_{obs}$ are only detected when $P_b$ values are

150    remarkably differentiated from $P_f$. Among NMR parameters, proton mono-selective longitudinal

151    relaxation rates ($R^{ms} = 1/T^{ms}$) are strongly responsive to complexation phenomena. Indeed they

152    undergo sharp increases when a molecule moves away from the fast-motion region, typical of small

153    molecules, to the slow-motion region ($\omega^2\tau_c^2 \gg 0.6$, where $\omega$ is the Larmor frequency and $\tau_c$ the

154  rotational correlation time), which is characteristic of small molecules bound to macromolecules. $R_i^{ms}$

155  is measured by selectively inverting the spin $i$ and following its magnetization recovery over time. By

156  contrast, the corresponding non-selective relaxation rates ($R_i^{ns} = 1/T_i^{ns}$), measured by simultaneous

157  inversion of the complete spins system, are scarcely sensitive to complexation (Niccolai and Valensin,

158  2012).

159  Cross-relaxation rate ($\sigma_{ij}$) between two spins $i$ and $j$ is another useful parameter to detect the slowing

160  down of molecular motion due to complexation phenomena. This parameter reflects the rate of

161  magnetization transfer between the magnetic moments of nuclei $i$ and $j$ at the distance $r_{ij}$. In the two

162  limit regions of fast motion ($\omega^2\tau_c^2 \ll 0.6$) and slow motion ($\omega^2\tau_c^2 \gg 0.6$), corresponding to the free

163  and bound states of the ligand respectively, the cross-relaxation term can be approximated to the

164  simple Equations (3) and (4):

165 
$$\sigma_{ij} = 0.5\ \gamma^4\ \hbar^2\ r_{ij}^{-6}\ \tau_c \qquad (\omega^2\tau_c^2 \ll 0.6) \tag{3}$$

166 
$$\sigma_{ij} = -0.1\ \gamma^4\ \hbar^2\ r_{ij}^{-6}\ \tau_c \qquad (\omega^2\tau_c^2 \gg 0.6) \tag{4}$$

167  Negative values of $\sigma_{ij}$ are characteristic of a slow-motion regime of the ligand induced by

168  macromolecule binding, while positive ones are associated to the fast-motion regime of a free ligand.

169  The cross-relaxation term can be calculated in a very simple way as the difference between bi-

170  selective ($R_{i,j}^{bs} = 1/T_{i,j}^{bs}$) and monoselective relaxation rates ($R_i^{ms}$, Eq. (5)). Bi-selective relaxation rates

171  are obtained by following the recovery of the spin $i$ under simultaneous inversion of the spins $i$ and $j$.

172 
$$\sigma_{ij} = R_{i,j}^{bs} - R_i^{ms} \tag{5}$$

173  Finally, among parameters which are remarkably responsive to complexation phenomena, the

174  diffusion coefficient ($D$, m$^2$s$^{-1}$) plays a leading role. It is a measure of the rate of translational

175  diffusion of a molecule in solution. Stokes-Einstein equation relates the hydrodynamic radius ($r_H$) and

176  solution viscosity ($\eta$) to the diffusion coefficient, which can be approximated in the form of Equation

177  (6) for spherical molecules:

178 
$$D = k_b T / (6\ \pi\ \eta\ r_H) \tag{6}$$

179    where $k_b$ is the Boltzmann constant, and $T$ is the absolute temperature.

180    Diffusion coefficients can be obtained by the NMR DOSY (Diffusion Ordered Spectroscopy)

181    technique (Evans et al., 2018; Pagès et al., 2017). Due to complexation phenomena, a decrease of the

182    ligand diffusion coefficient is expected as a consequence of the increased apparent size in its bound

183    form.

184

185    *3.2. MCD characterization*

186    The complete NMR characterization of the cyclodextrin was performed. In the ^{1}H NMR spectral

187    region between 4.94 ppm and 5.13 ppm (Figure 3) two broad resonances were detected for the

188    anomeric protons, which were identified on the basis of their heteronuclear correlation (HSQC map)

189    with ^{13}C carbon nuclei at 101.6 ppm and 99.1 ppm, respectively (Figure S1, Supplementary material).
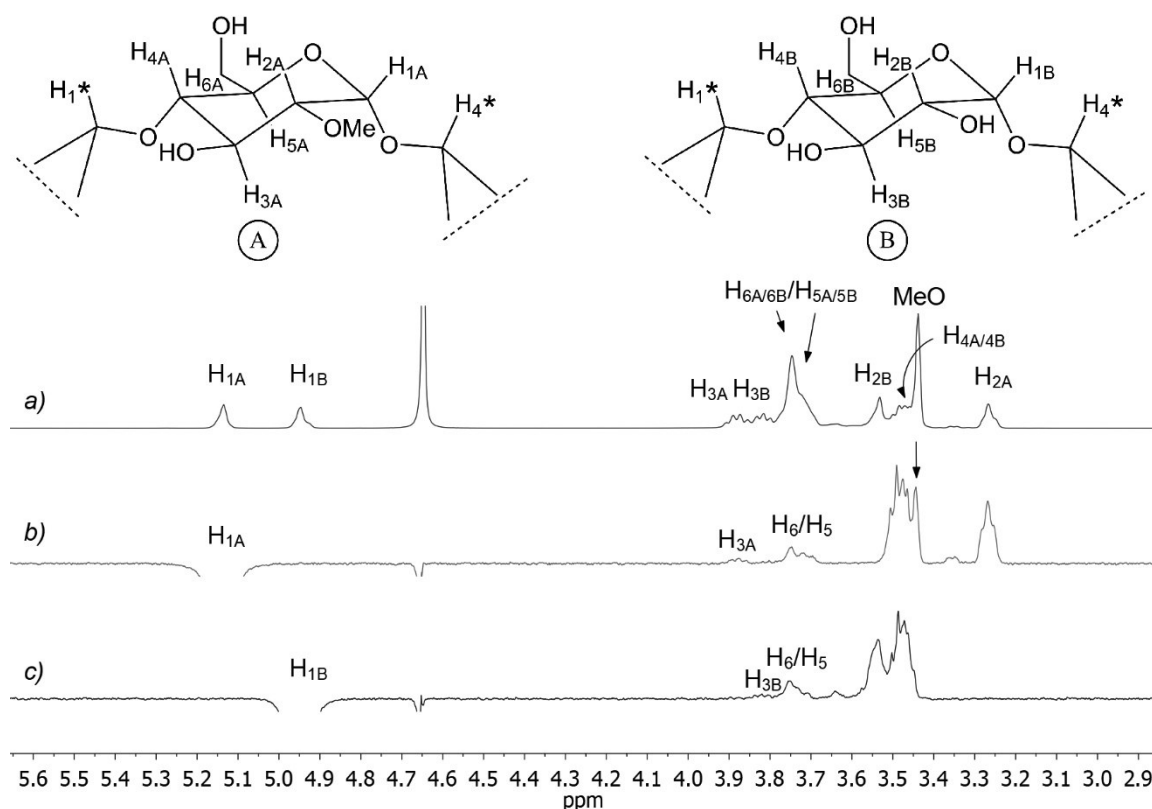


190

191   Figure 3. $^1$H NMR spectrum (600 MHz, 15 mM, D$_2$O, 25 °C) of MCD (a); 1D ROESY spectra of

192   MCD corresponding to the perturbation of H$_{1A}^{MCD}$ (b) and H$_{1B}^{MCD}$ (c). * refers to protons belonging to

193   the adjacent glucose units.


194   The high-frequency shifted anomeric proton resonance at 5.13 ppm (H$_{1A}^{MCD}$) was attributed to the

195   units bearing a methyl group at C$_{2A}^{MCD}$ site (A unit), since their selective perturbation produced

196   through space dipolar interaction at the frequency of methoxy protons, as shown in the 1D ROESY

197   spectrum (Figure 3b). On the contrary, low-frequency shifted anomeric proton at 4.94 ppm (H$_{1B}^{MCD}$)

198   did not produce any ROE at the methoxy proton frequency (Figure 3c) and was assigned to units

199   which have free -OH group at C$_{2B}^{MCD}$ (B unit). The ratio of integrated areas of the two anomeric

200   protons H$_{1A}^{MCD}$ and H$_{1B}^{MCD}$, and the comparison of integrated area of the anomeric protons and of the

201   remaining ring and methoxy resonances (4.0÷3.2 ppm) confirmed that the average number of

202   methoxy groups per anhydroglucose unit was 0.5.


203

204   ROESY and TOCSY experiments supported the complete assignment of the resonances of the two

205   kinds of units, substituted (A) and unsubstituted (B), and $^1$H NMR spectral data are summarized in

206   Table 1. Interestingly, NMR parameters of the B unit were quite similar to those of underivatized β-

207   cyclodextrin (Table 1).


208

209   Table 1. $^1$H chemical shifts (ppm) of MCD and β-CD protons (600 MHz, 15 mM, D$_2$O, 25 °C).

|            | MCD (A unit) | MCD (B unit) | β-CD |
|------------|--------------|--------------|------|
| H$_1$      | 5.13         | 4.94         | 4.94 |
| H$_2$      | 3.26         | 3.53         | 3.52 |
| H$_3$      | 3.88         | 3.81         | 3.84 |
| H$_4$      | 3.48         | 3.45         | 3.46 |
| H$_5$      | 3.70         | 3.73         | 3.74 |
| H$_{6/6'}$ | 3.74         | 3.74         | 3.75 |

210

211　One aspect to be taken into consideration when dealing with cyclodextrin derivatives is the impact of

212　derivatization on the conformational features of the cyclodextrin, which, in turn, may potentially

213　affect its complexing properties. In particular, severe deviations from the truncated cone shape, which

214　is peculiar of native β-cyclodextrin, have been evidenced as the consequence of hydroxyl

215　derivatization (Uccello-Barretta et al., 2005). In some limit cases also conformational transitions of

216　single glucopyranose units from chair to twisted forms have been detected (Uccello-Barretta et al.,

217　1997). Such a kind of effects could perturbate the balance between polarity of the external surface and

218　apolarity of the internal cavity.

219　Deviations from the truncated cone shape may originate from rotations about glycosidic linkages

220　connecting units each other, which change the distance between the $H_1^{MCD}$ and $H_{4*}^{MCD}$ protons of

221　adjacent glucopyranose units (* refers to protons belong to the adjacent glucose units, see Figure 3)

222　with respect to intra-ring fixed distance between the protons $H_1^{MCD}$ and $H_2^{MCD}$ on the same unit. It

223　simultaneously brings anomeric proton $H_1^{MCD}$ of one unit in proximity of internal protons $H_{3*}^{MCD}$ or

224　$H_{5*}^{MCD}$ of the adjacent one (Figure 3). ROE experiments are remarkably useful in investigating above-

225　mentioned effects (Uccello-Barretta et al., 2005, 1997).

226　In our case, partial superimposition between $H_2^{MCD}$ and $H_4^{MCD}$ resonances of the two units did not

227　allow us to give a univocal interpretation of the relative intensities of $H_1^{MCD}$-$H_2^{MCD}$ and $H_1^{MCD}$-$H_{4*}^{MCD}$

228　ROEs.

229　Taking into account that rotations about the glycosidic linkages lead $H_1^{MCD}$ protons of one

230　glucopyranose unit in proximity of $H_3^{MCD}$ and $H_5^{MCD}$ internal protons of adjacent one (Figure S2,

231　Supplementary material), we looked for eventual inter-units $H_1^{MCD}$ - $H_{3*}^{MCD}$ and $H_1^{MCD}$ - $H_{5*}^{MCD}$ ROE

232　effects, the intensities of which were instead very low (1D ROESY experiments of Figure 3b,c).

233　Therefore, a very low degree of rotation about glycosidic linkages occurs. Low molar substitution

234　(0.5) remarkably improves cyclodextrin solubility (200 mg/mL in comparison with 18 mg/mL for β-

235　CD), but does not bring about significant deviations from the truncated cone shape of the cyclodextrin

236　and, hence, its complexing properties are preserved.

237

## 3.3. PN characterization

$^1$H NMR resonances of PN (Figure 4) were assigned to the corresponding nuclei by accurate comparison of 2D COSY, TOCSY, HSQC maps (Figures S3-S5, Supplementary material) and 1D ROESY spectra.
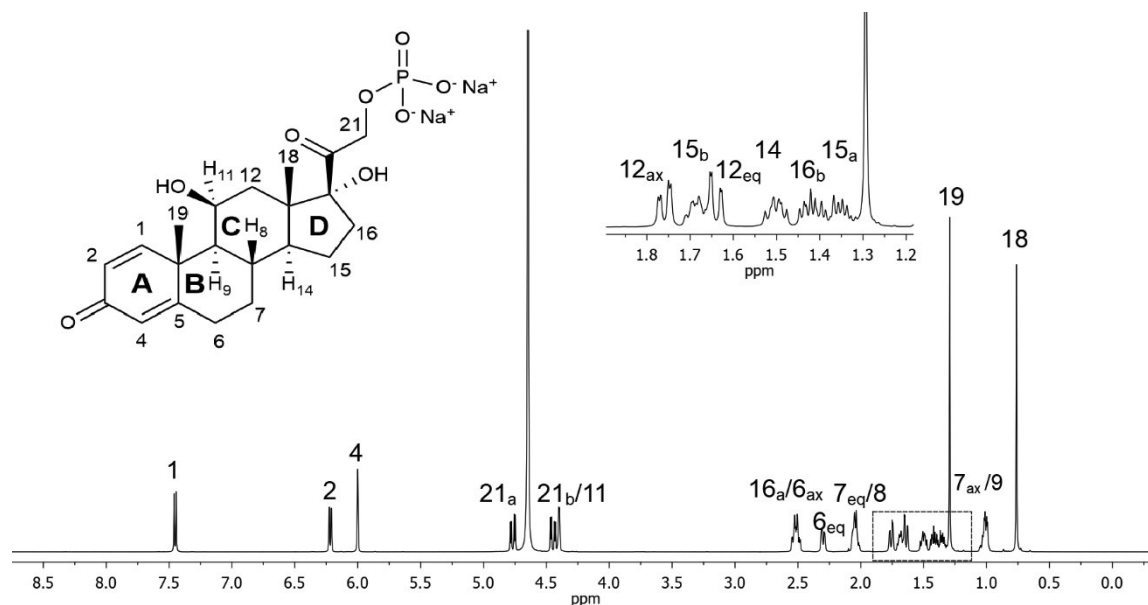


Figure 4. $^1$H NMR spectrum (600 MHz, 15 mM, $D_2O$, 25 °C) of PN.

243

The analysis of PN conformational features deals with possible distortions of its six- and five-membered rings (B, C, and D rings), as well as the determination of the preferential arrangement of the side chain with respect to the rigid backbone. ROE effects between the protons of methyl groups $Me_{18}^{PN}$ and $Me_{19}^{PN}$ were detected (Figure 5a,b) confirming their cisoid arrangement.
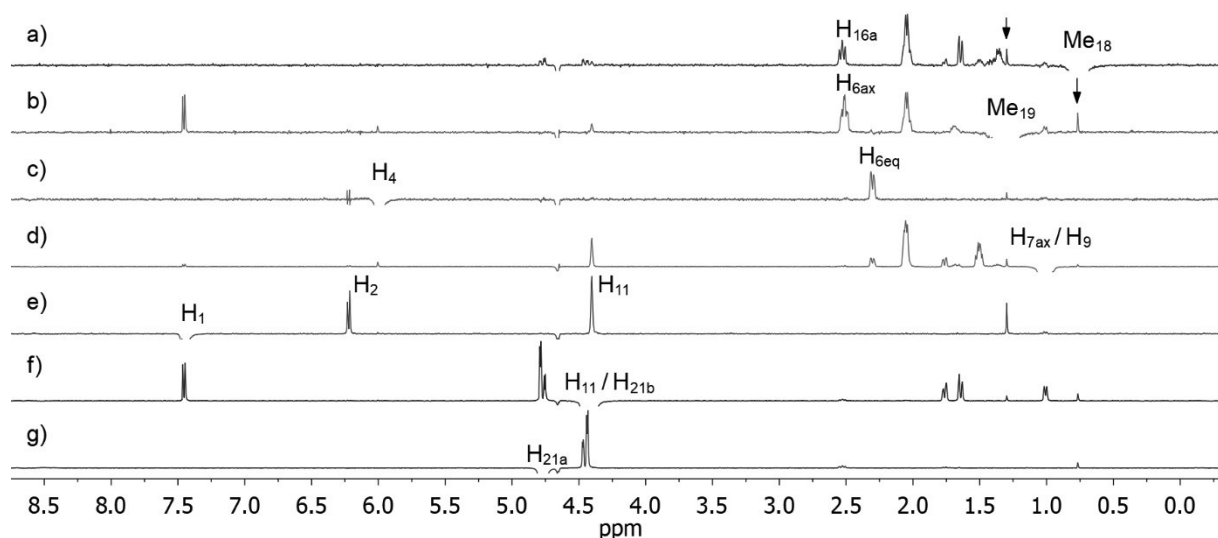
Figure 5. 1D ROESY spectra (600 MHz, 15 mM, $D_2O$, 25 °C) of PN corresponding to the perturbation of $Me_{18}^{PN}$ (a), $Me_{19}^{PN}$ (b), $H_4^{PN}$ (c), $H_{7ax}^{PN}/H_9^{PN}$ (d), $H_1^{PN}$ (e), $H_{11}^{PN}/H_{21b}^{PN}$ (f), and $H_{21a}^{PN}$ (g).

$H_4^{PN}$ proton of ring A produces ROE interaction exclusively with one of the two protons at the $C_6^{PN}$ site of B ring (2.30 ppm, Figure 5c), which must lay parallel to the plane of A ring and, hence, pseudo-equatorial ($H_{6eq}^{PN}$). The other methylene proton at 2.50 ppm lies perpendicular to A plane, in a way to produce dipolar interactions with protons lying on the surface of the compound containing $Me_{19}^{PN}$ (Figure 5b). One of the two protons $H_7^{PN}$ (1.01 ppm) does not give ROE at the frequency of $H_{6ax}^{PN}$ and, hence, is itself in axial arrangement ($H_{7ax}^{PN}$, Figure 5d).

Conformational preference at C ring was clearly pointed out by the ROE produced by $H_1^{PN}$ proton of A ring (Figure 5e). In particular, comparable inter-ROEs $H_1^{PN}$-$H_2^{PN}$ and $H_1^{PN}$-$H_{11}^{PN}$ were detected which demonstrated the equatorial arrangement of $H_{11}^{PN}$. Therefore, -OH group is axial and bent at $Me_{19}^{PN}$. The magnitude of dipolar interactions between proton $H_{11}^{PN}$ and the two protons $H_{12}^{PN}$ are comparable (Figure 5f) as expected if $C_{11}^{PN}$- $H_{11}^{PN}$ bond bisects the angle formed by the two protons $H_{12}^{PN}$ and $C_{12}^{PN}$, with the equatorial one (1.64 ppm) bent towards the -OH group (Figure 6). Extensive superimposition between protons at $C_{15}^{PN}$ and $C_{16}^{PN}$ sites did not allow to give univocal interpretation of ROE effects and, hence, information about D ring. Lateral chain must be freely rotating far away

13

266    from the rigid backbone since it did not produce any dipolar interactions with protons of C or D rings

267    (Figure 5g). Strong chemical shift differentiation of methylene protons $H_{21}$ is to be attributed to

268    anisotropic effects produced by the adjacent carbonyl function.

269
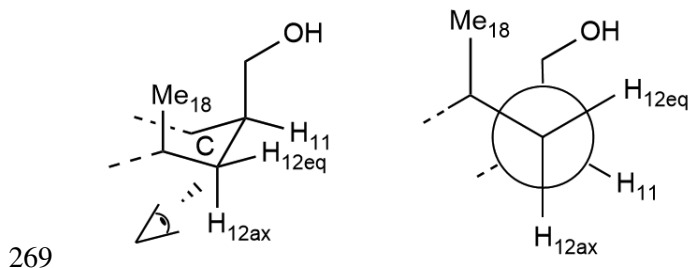


270    Figure 6. Stereochemical representation of $C_{11}^{PN}$-$C_{12}^{PN}$ fragment of PN ring C by chair and Newman

271    structure.

272

273    *3.4. PN/MCD stereochemical model*

274    The presence of MCD produced notable variations in PN chemical shifts (Table 2). Complexation

275    shifts ($\Delta\delta=\delta_{mixture}-\delta_{free}$, ppm) were remarkably high for protons of rings B and C, which were on the

276    same side of the rigid backbone bearing the hydroxyl function, i.e. protons $H_{12ax}^{PN}$ (0.12 ppm), $Me_{19}^{PN}$

277    (0.14 ppm), $H_{7eq}^{PN}$ (0.13 ppm), $H_{6ax}^{PN}$ (0.16 ppm) and $H_8^{PN}$ (0.12 ppm). This selectivity for one face of

278    the polycyclic system suggests that -OH group of the guest is extensively involved in hydrogen bond

279    interactions with hydroxyls at the rims of the cyclodextrin thus shortening the distance between host

280    and guest nuclei facing at -OH group of PN. Protons belonging to the conjugated carbonyl function of

281    ring A, and to the 5-membered ring at the other end of PN (ring D) are relatively less affected with

282    $|\Delta\delta|=0.01\div0.05$ ppm. Interestingly, differentiated complexation shifts were measured for the two

283    protons $H_{21a}^{PN}$ and $H_{21b}^{PN}$ of the side chain.

14

284     Table 2. $^1$H NMR complexation shifts ($\Delta\delta$, ppm) of PN protons (15 mM) in 1:1 PN/MCD mixture

285     (600 MHz, $D_2O$, 25 °C).

| PN | | | | | |
|------|--------|-------------|------|-------------|-------------|
| Ring | Proton | $\Delta\delta$ | Ring | Proton | $\Delta\delta$ |
| A | $H_1$ | 0.00 | C | $H_{11}$ | 0.03 |
| A | $H_2$ | -0.05 | C | $H_{12eq}$ | 0.08 |
| A | $H_4$ | -0.05 | C | $H_{12ax}$ | 0.12 |
| A/B | $Me_{19}$ | 0.14 | C/D | $Me_{18}$ | 0.05 |
| B | $H_{6ax}$ | 0.16 | C/D | $H_{14}$ | 0.02 |
| B | $H_{6eq}$ | 0.09 | D | $H_{15a}$ | 0.03 |
| B | $H_{7ax}$ | 0.03 | D | $H_{15b}$ | 0.04 |
| B | $H_{7eq}$ | 0.13 | D | $H_{16a}$ | 0.02 |
| B/C | $H_8$ | 0.12 | D | $H_{16b}$ | 0.02 |
| B/C | $H_9$ | -0.09 | - | $H_{21a}$ | 0.04 |
| | | | - | $H_{21b}$ | 0.01 |

286

287     Regarding host protons, the ones lying in the internal cavity of MCD ($H_3^{MCD}$ and $H_5^{MCD}$), showed

288     remarkable complexation shifts ($|\Delta\delta|$=0.14÷0.19 ppm, Table 3), with no sharp preference for one kind

289     of glucopyranose unit with respect to the other (i.e. methylated *vs* non-methylated) or for the wider

290     part of the cavity (that one bearing protons $H_3^{MCD}$) with respect to the narrower one having protons

291     $H_5^{MCD}$ on it (Table 3). Protons located at the external surface of the cyclodextrin were affected by the

292     guest to a less extent.

293    Table 3. $^1$H NMR complexation shifts ($\Delta\delta$, ppm) of MCD protons (15 mM) in 1:1 PN/MCD mixture

294    (600 MHz, D$_2$O, 25 °C).

| MCD | | | |
|---|---|---|---|
| Proton | $\Delta\delta$ | Proton | $\Delta\delta$ |
| H$_{1A}$ | -0.03 | H$_{1B}$ | -0.01 |
| H$_{2A}$ | 0.02 | H$_{2B}$ | 0.02 |
| H$_{3A}$ | -0.15 | H$_{3B}$ | -0.14 |
| H$_{4A}$ | 0.01 | H$_{4B}$ | 0.02 |
| H$_{5A}$ | -0.16 | H$_{5B}$ | -0.19 |
| H$_{6A}$ | 0.00 | H$_{6B}$ | 0.00 |
| MeO | 0.02 | | |

295

296    Such a kind of behaviour let us to conclude that PN could be very deeply included into the

297    cyclodextrin with the two ends of PN protruding from narrow (ring A) and wide (ring D) rims of the

298    cyclodextrin, which is only expected for cases of very high host-guest affinity.

299    The relative stereochemistry of the host and the guest in the inclusion complex was clearly ascertained

300    by an accurate analysis of inter-molecular ROEs. Starting from PN ring A bearing the carbonyl

301    function, the analysis of 1D ROESY spectra of H$_2^{PN}$ and H$_4^{PN}$ (Figure 7a,b) showed higher dipolar

302    correlation with H$_{5A}^{MCD}$/H$_{5B}^{MCD}$ protons located at the narrow rim than those with H$_{3A}^{MCD}$/H$_{3B}^{MCD}$,

303    located at the wide rim. On the contrary, protons H$_1^{PN}$ of A ring (Figure 7c) and protons at B ring

304    (Figure S6, Supplementary material) produced progressively increasing ROEs at H$_3^{MCD}$ protons of

305    both units of MCD. Intermolecular effects vanished going towards protons of C and D rings, as well

306    as for the polar lateral chain.

307
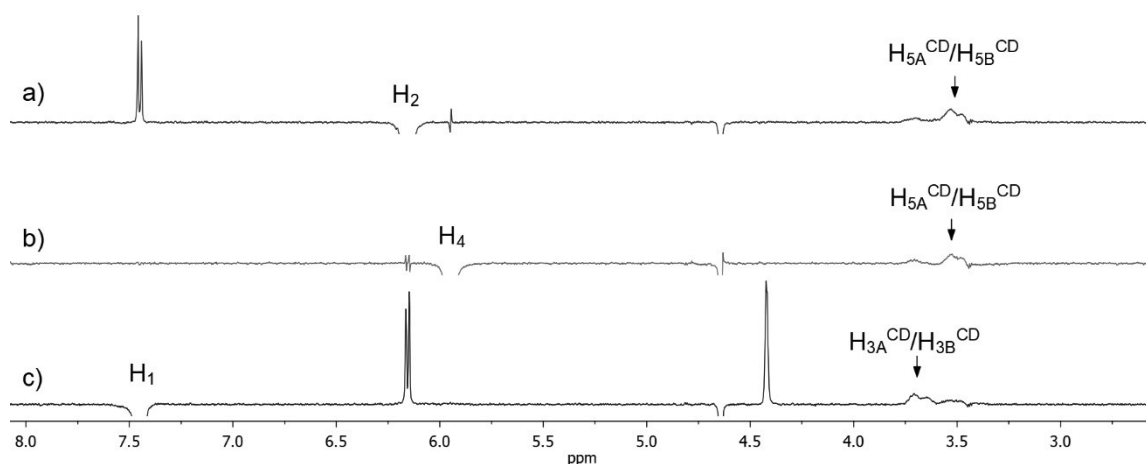
Figure 7. 1DROESY spectra (600 MHz, 15 mM, D$_2$O, 25 °C) of PN/MCD 1:1 mixture corresponding to the perturbation of H$_2^{PN}$ (a), H$_4^{PN}$ (b), and H$_1^{PN}$ (c).

Therefore it can be concluded that the interaction of PN with MCD originated from a deep inclusion of PN inside the cyclodextrin cavity, with ring A protruding out of the narrow rim and rings C, D and the lateral arm protruding from the wide part of the cavity, with -OH group at C$_{11}^{PN}$ interacting with the hydroxyl at the wide rim of the cyclodextrin (Figure 8).
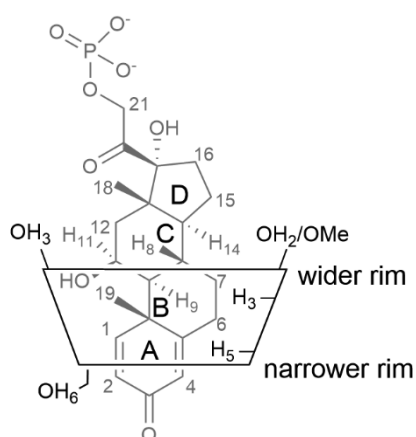


Figure 8. Graphical representation of PN inclusion mode inside MCD.

The effect of complexation on the diffusion coefficients of PN and MCD supports the occurrence of strong host-guest interactions. As a matter of fact, PN faces a relevant slowing down of its

320  translational motion when compared as pure ($3.8 \times 10^{-10}$ m$^2$s$^{-1}$) or in mixture with MCD ($2.9 \times 10^{-10}$

321  m$^2$s$^{-1}$). The diffusion coefficient of MCD is affected to a less extent from $2.7 \times 10^{-10}$ m$^2$s$^{-1}$ to $2.2 \times 10^{-10}$

322  m$^2$s$^{-1}$, because of the fact that guest tends to follow the translational diffusion of the host (Table 4).

323

324  Table 4. Diffusion coefficients ($D$, m$^2$s$^{-1}$) of the selected compounds (15 mM) in 1:1 PN/MCD

325  mixture (600 MHz, D$_2$O, 25 °C).

| | $D$ ($\times 10^{10}$) | |
|---|---|---|
| | PN | MCD |
| Pure | 3.8±0.1 | 2.7±0.1 |
| Mixture (1:1) | 2.9±0.1 | 2.2±0.1 |

326

### 3.5. Polymers Characterization

328  On the basis of a consolidated quantitative $^1$H NMR protocol developed for the characterization of

329  modified chitosans (Cesari et al., 2020b), N$^+$-rCh was fully characterized, with degrees of acetylation

330  of 8.8%, degree of derivatization of 42.4%, and quaternary to neutral nitrogen ratio of the modified

331  chains of 2.3. It roughly corresponded to a polymer with an average of 600 monomeric units per N$^+$-

332  Ch chain. Cyclodextrin content of 52 w/w% was calculated for N$^+$-rCh-MCD, by using pure MCD as

333  external standard. Then, from the integrated areas of opportune $^1$H NMR sub-regions (Figure S7,

334  Supplementary material) the amount of linker was calculated (31% w/w%) (Cesari et al., 2020b).

335  Molar ratio between MCD/linker (1:4) indicated a relevant amount of linker bound to polymer but not

336  capped with MCD.

337

338    *3.6. Affinity of PN towards $N^+$-rCh-MCD*

339    To better understand how the covalent conjugation of MCD grafted to polymeric backbone could

340    affect binding ability of polymeric receptors, binding affinity of PN towards the model cyclodextrin

341    MCD and the two polymeric systems, i.e. the parent chitosan $N^+$-rCh and its cyclodextrin conjugate

342    $N^+$-rCh-MCD, were compared by analysing binary mixtures PN/MCD, PN/$N^+$-rCh, and PN/$N^+$-rCh-

343    MCD. Furthermore, the ternary system PN/MCD/$N^+$-rCh, containing the physical mixture of MCD

344    and the parent chitosan ($N^+$-rCh), was also considered. As NMR parameters highly responsive to

345    binding processes, proton selective relaxation rates of PN were measured in the different mixtures and

346    compared with the pure compound PN. Among observable PN proton nuclei, protons $H_1^{PN}$, $H_2^{PN}$, and

347    $H_4^{PN}$ of ring A were selected, since their resonances were comprised in the high-frequency spectral

348    region, with no interferences from resonances of the polymer or cyclodextrin.

349    Possible effects on relaxation parameters due to viscosity changes were ruled out by using

350    tetramethylsilane (TMS) as internal standard, added as DMSO solution. Its relaxation rate was

351    compared in $D_2O$/DMSO (95:5) solution, with and without binary/ternary mixtures. The same

352    relaxation rate (0.15 $s^{-1}$) was measured in all the solutions. In that way relaxation rates changes have

353    been univocally attributed to binding effects.

354    Low water solubility of $N^+$-rCh-MCD (about 3.5 mg/mL) limited the choice of concentration values

355    for the analysis of the mixtures. Therefore, measurements were performed by using 3.11 mg/mL of

356    $N^+$-rCh-MCD and, on the basis of the knowledge of cyclodextrin content in the polymer, PN

357    concentration (0.66 mg/mL) was selected to be equimolar with respect to MCD. The weight amount

358    of chitosan was kept constant (1.49 mg/mL) in the mixtures containing $N^+$-rCh and MCD/$N^+$-rCh, and

359    equal to that determined for $N^+$-rCh-MCD at the selected concentration.

360    In spite of the very low PN concentration, the presence of the cyclodextrin in the equimolar binary

361    mixture PN/MCD brought about a 2-fold increase of relaxation rates of PN in comparison with the

362    pure compound (Table 5). Proton selective relaxation rates changed from 0.98 $s^{-1}$ to 1.26 $s^{-1}$ for $H_1^{PN}$,

363    from 0.36 $s^{-1}$ to 0.68 $s^{-1}$ for $H_2^{PN}$ and from 0.44 $s^{-1}$ to 0.79 $s^{-1}$ for $H_4^{PN}$.

Table 5. Mono-selective relaxation rates ($R^{ms}$, s$^{-1}$) of $H_1^{PN}$, $H_2^{PN}$, and $H_4^{PN}$ protons (600 MHz, D$_2$O, 25 °C) in different mixtures (PN 0.66 mg/mL, MCD 1.62 mg/mL, N$^+$-rCh 1.49 mg/mL, N$^+$-rCh-MCD 3.11 mg/mL).

| | $R^{ms}$ | | |
|---|---|---|---|
| | $H_1^{PN}$ | $H_2^{PN}$ | $H_4^{PN}$ |
| PN | 0.98±0.01 | 0.36±0.01 | 0.44±0.01 |
| PN/MCD 1:1 | 1.26±0.02 | 0.68±0.02 | 0.79±0.01 |
| PN/N$^+$-rCh | 3.04±0.09 | 1.31±0.02 | 1.61±0.03 |
| PN/MCD/N$^+$-rCh | 2.74±0.07 | 1.30±0.01 | 1.61±0.03 |
| PN/N$^+$-rCh-MCD | 29.69±1.57 | 17.26±0.69 | 18.61±1.14 |

PN proton nuclei underwent higher increases in the presence of the precursor ammonium chitosan since the values of 3.04 s$^{-1}$, 1.31 s$^{-1}$ and 1.61 s$^{-1}$ were measured for $H_1^{PN}$, $H_2^{PN}$, and $H_4^{PN}$, respectively in the binary mixture PN/N$^+$-rCh.

Interestingly, co-presence of the cyclodextrin and the ammonium chitosan in the ternary physical mixture PN/MCD/N$^+$-rCh did not produce additive effects on PN proton selective relaxation rates, since they were almost unchanged in comparison with the binary mixture PN/N$^+$-rCh: probably, at such a low PN concentration (0.66 mg/mL corresponding to 1.4 mM to be compared with 15 mM, employed to investigate PN to MCD interaction) a privileged interaction with the polymeric backbone occurs subtracting PN from its interaction with MCD. Affinity of PN towards N$^+$-rCh is higher, as expected for the higher contact surface granted by the polymer, and possibly by an interaction through PN negatively charged phosphate group.

Interestingly, outstanding variations of PN relaxation parameters were recorded in the mixture PN/N$^+$-rCh-MCD, reaching increment of 30 times respect to pure PN. Remarkably higher binding ability of polymer covalently conjugated to the cyclodextrin with respect to its ammonium precursor was confirmed by analysis of cross-relaxation parameter for the proton pair $H_1^{PN}$/$H_2^{PN}$ (Table 6), which

383  changed from 0.01 s$^{-1}$ for pure PN to -0.81 s$^{-1}$ for PN/N$^+$-rCh and -10.13 s$^{-1}$ for PN/N$^+$-rCh-MCD,

384  reflecting the progressive increases of rotational correlation times of the vector connecting the two

385  protons.

386

387  Table 6. Cross-relaxation parameter of $H_1^{PN}$/$H_2^{PN}$ proton pair ($\sigma_{12}$, s$^{-1}$) of PN as pure (0.66 mg/mL)

388  and in the presence of N$^+$-rCh (1.49 mg/mL) or N$^+$-rCh-MCD (3.11 mg/mL).

|  | $\sigma_{12}$ |
| --- | --- |
| PN | 0.01±0.04 |
| PN/N$^+$-rCh | -0.81±0.15 |
| PN/N$^+$-rCh-MCD | -10.13±2.94 |

389

390  **4. Conclusions**

391  Covalent grafting of cyclodextrins onto ammonium chitosans backbone affords mucoadhesive and

392  biocompatible materials with improved binding ability towards lipophilic (Piras et al., 2018b, 2018a),

393  and hydrophilic (Cesari et al., 2020b) active ingredients. Their protecting role against degradative

394  processes has been also demonstrated (Cesari et al., 2020b). Remarkable affinity of N$^+$-rCh-MCD

395  towards PN, an amphiphilic compound, has been here highlighted by exploiting enormous

396  potentialities of NMR spectroscopy in the investigation of supramolecular aggregation phenomena.

397  The use of methylated β-cyclodextrin with a low substitution degree brings about a remarkable water

398  solubility without producing significant deformations of the truncated cone shape which is typical of

399  less soluble parent β-cyclodextrin.

400  Hydrophilic hydrogen bond interactions between -OH groups of PN and MCD reasonably occur at the

401  wide rim of the cyclodextrin, driving the deep inclusion of A and B moieties of PN into the apolar

402  cavity of the cyclodextrin. As a result of PN complexation into the cyclodextrin, polar flexible arm of

403  the steroid remains available for electrostatic interactions with cationic pendants on the chitosan

404 backbone, synergistic effect of which only arises when a covalent grafting is exploited. This unique

405 feature cannot be reproduced by the simple physical mixture PN/MCD/N$^+$-rCh.

406 The outstanding affinity found for N$^+$-rCh-MCD polymeric platform can be exploited in drugs

407 formulation as an alternative strategy to the nanoparticles production, avoiding the time-consuming

408 optimization of production protocols.

409

412

413 **References**

414 Cesari, A., Fabiano, A., Piras, A.M., Zambito, Y., Uccello-Barretta, G., Balzano, F., 2020a.

415      Binding and mucoadhesion of sulfurated derivatives of quaternary ammonium-

416      chitosans and their nanoaggregates: An NMR investigation. J. Pharm. Biomed. Anal.

417      177, 112852. https://doi.org/10.1016/j.jpba.2019.112852

418 Cesari, A., Recchimurzo, A., Fabiano, A., Balzano, F., Rossi, N., Migone, C., Uccello-

419      Barretta, G., Zambito, Y., Piras, A.M., 2020b. Improvement of Peptide Affinity and

420      Stability by Complexing to Cyclodextrin-Grafted Ammonium Chitosan. Polymers 12,

421      474. https://doi.org/10.3390/polym12020474

422 Dash, M., Chiellini, F., Ottenbrite, R.M., Chiellini, E., 2011. Chitosan—A versatile semi-

423      synthetic polymer in biomedical applications. Prog. Polym. Sci. 36, 981–1014.

424      https://doi.org/10.1016/j.progpolymsci.2011.02.001

425 Davis, M.E., Brewster, M.E., 2004. Cyclodextrin-based pharmaceutics: past, present and

426      future. Nat. Rev. Drug Discov. 3, 1023–1035. https://doi.org/10.1038/nrd1576

427     Evans, R., Dal Poggetto, G., Nilsson, M., Morris, G.A., 2018. Improving the Interpretation of

428          Small Molecule Diffusion Coefficients. Anal. Chem. 90, 3987–3994.

429          https://doi.org/10.1021/acs.analchem.7b05032

430     Fabiano, A., Piras, A.M., Uccello-Barretta, G., Balzano, F., Cesari, A., Testai, L., Citi, V.,

431          Zambito, Y., 2018. Impact of mucoadhesive polymeric nanoparticulate systems on

432          oral bioavailability of a macromolecular model drug. Eur. J. Pharm. Biopharm. 130,

433          281–289. https://doi.org/10.1016/j.ejpb.2018.07.010

434     Freeman, R., Wittekoek, S., 1969. Selective determination of relaxation times in high

435          resolution NMR. J. Magn. Reson. 1969 1, 238–276. https://doi.org/10.1016/0022-

436          2364(69)90065-1

437     Miao, T., Wang, J., Zeng, Y., Liu, G., Chen, X., 2018. Polysaccharide-Based Controlled

438          Release Systems for Therapeutics Delivery and Tissue Engineering: From Bench to

439          Bedside. Adv. Sci. 5, 1700513. https://doi.org/10.1002/advs.201700513

440     Niccolai, Valensin, 2012. Advanced Magnetic Resonance Techniques in Systems of High

441          Molecular Complexity. Birkhauser Verlag GmbH Springer, CH-4055 Basel;

442          Secaucus.

443     Pagès, G., Gilard, V., Martino, R., Malet-Martino, M., 2017. Pulsed-field gradient nuclear

444          magnetic resonance measurements (PFG NMR) for diffusion ordered spectroscopy

445          (DOSY) mapping. The Analyst 142, 3771–3796.

446          https://doi.org/10.1039/C7AN01031A

447     Piras, A.M., Fabiano, A., Chiellini, F., Zambito, Y., 2018a. Methyl-β-cyclodextrin quaternary

448          ammonium chitosan conjugate: nanoparticles vs macromolecular soluble complex.

449          Int. J. Nanomedicine Volume 13, 2531–2541. https://doi.org/10.2147/IJN.S160987

450     Piras, A.M., Zambito, Y., Burgalassi, S., Monti, D., Tampucci, S., Terreni, E., Fabiano, A.,

451          Balzano, F., Uccello-Barretta, G., Chetoni, P., 2018b. A water-soluble, mucoadhesive

quaternary ammonium chitosan-methyl-β-cyclodextrin conjugate forming inclusion complexes with dexamethasone. J. Mater. Sci. Mater. Med. 29. https://doi.org/10.1007/s10856-018-6048-2

Rautio, J., Kumpulainen, H., Heimbach, T., Oliyai, R., Oh, D., Järvinen, T., Savolainen, J., 2008. Prodrugs: design and clinical applications. Nat. Rev. Drug Discov. 7, 255–270. https://doi.org/10.1038/nrd2468

Saokham, P., Muankaew, C., Jansook, P., Loftsson, T., 2018. Solubility of Cyclodextrins and Drug/Cyclodextrin Complexes. Molecules 23, 1161. https://doi.org/10.3390/molecules23051161

Sogias, I.A., Khutoryanskiy, V.V., Williams, A.C., 2010. Exploring the Factors Affecting the Solubility of Chitosan in Water. Macromol. Chem. Phys. 211, 426–433. https://doi.org/10.1002/macp.200900385

Sreekumar, S., Goycoolea, F.M., Moerschbacher, B.M., Rivera-Rodriguez, G.R., 2018. Parameters influencing the size of chitosan-TPP nano- and microparticles. Sci. Rep. 8, 4695. https://doi.org/10.1038/s41598-018-23064-4

Uccello-Barretta, G., Cuzzola, A., Balzano, F., Menicagli, R., Iuliano, A., Salvadori, P., 1997. A New Stereochemical Model from NMR for Benzoylated Cyclodextrins, Promising New Chiral Solvating Agents for the Chiral Analysis of 3,5-Dinitrophenyl Derivatives. J. Org. Chem. 62, 827–835. https://doi.org/10.1021/jo961562x

Uccello-Barretta, G., Sicoli, G., Balzano, F., Salvadori, P., 2005. NMR spectroscopy: a powerful tool for detecting the conformational features of symmetrical persubstituted mixed cyclomaltoheptaoses (β-cyclodextrins). Carbohydr. Res. 340, 271–281. https://doi.org/10.1016/j.carres.2004.11.022

Zambito, Y., Zaino, C., Uccello-Barretta, G., Balzano, F., Di Colo, G., 2008. Improved synthesis of quaternary ammonium-chitosan conjugates (N+-Ch) for enhanced

24

477    intestinal drug permeation. Eur. J. Pharm. Sci. 33, 343–350.

478    https://doi.org/10.1016/j.ejps.2008.01.004

479 Zhang, J., Xia, W., Liu, P., Cheng, Q., Tahi, T., Gu, W., Li, B., 2010. Chitosan Modification

480    and Pharmaceutical/Biomedical Applications. Mar. Drugs 8, 1962–1987.

481    https://doi.org/10.3390/md8071962

482

**\*Conflict of Interest**

**Declaration of interests**

☒ The authors declare that they have no known competing financial interests or personal relationships that could have appeared to influence the work reported in this paper.

☐The authors declare the following financial interests/personal relationships which may be considered as potential competing interests:

# Credit Author Statement

2-Methyl-β-cyclodextrin grafted ammonium chitosan: synergistic effects of cyclodextrin host and polymer backbone in the interaction with amphiphilic prednisolone phosphate salt as revealed by NMR spectroscopy

Andrea Cesari, Anna Maria Piras, Ylenia Zambito, Gloria Uccello Barretta, and Federica Balzano*

Andrea Cesari: Methodology, Formal Analysis, Investigation, Writing-Original Draft, Visualization
Anna Maria Piras: Writing-Review & Editing, Supervision
Ylenia Zambito: Writing-Review & Editing, Supervision
Gloria Uccello Barretta: Conceptualization, Methodology, Validation, Writing-Review & Editing, Project administration, Supervision, Funding acquisition
Federica Balzano: Conceptualization, Methodology, Validation, Writing-Review & Editing, Project administration, Supervision

**Supplementary Material**

**Click here to download Supplementary Material: Balzano-Cesari_Supporting Material-revised.docx**